

Tailoring Pure Inorganic Electrolyte for Aqueous Sodium-Ion Batteries Operating at -60°C

Kunjie Zhu,^[b] Zhiqin Sun,^[b] Ting Jin,^[b] Xuchun Chen,^[b] Yuchang Si,*^[a] Haixia Li,^[b] and Lifang Jiao*^[b]

Aqueous sodium-ion batteries (ASIBs) have attracted increasing attention for next-generation energy storage technologies due to their abundant resources and environmentally-safe, while their application scenarios are severely limited by the high freezing point of conventional aqueous electrolytes. To overcome the aforementioned issues of ASIBs, a novel hybrid 3.5 m $\text{Mg}(\text{ClO}_4)_2 + 0.5 \text{ m NaClO}_4$ electrolyte (m: mol kg^{-1}) with an ultra-low freezing point ($<-80^{\circ}\text{C}$) is proposed. The exceptional anti-freezing feature is mainly attributed to the higher ionic potential of Mg^{2+} , greatly affecting the chemical environment of water molecules and inhibiting ice formation under subzero

conditions. Benefiting from the superiority of ionic conductivity (4.86 mScm^{-1}) for the hybrid electrolyte at -60°C , the full cell of active carbon | $\text{NaTi}_2(\text{PO}_4)_3@\text{C}$ delivers an ultra-long lifespan of 10000 cycles under 8 C (1 C = 133 mA g^{-1}) at -60°C . More importantly, some representative devices in daily life including smartphone and motor can be powered by ASIBs at -60°C . Therefore, this work provides a rational and effective strategy for design and application of ASIBs with excellent electrochemical performance that can work in extremely cold environments.

Introduction

With the similar energy storage mechanism to commercial lithium-ion batteries, aqueous sodium-ion batteries (ASIBs) have some unique advantages including high security, low cost, ultrafast diffusion kinetics and manufacturing efficiency, which are regarded as promising candidates for the next generation grid-scale energy storage.^[1] However, the intrinsic feature of relatively-high freezing point for conventional aqueous electrolytes causes the electrochemical performance deterioration of ASIBs under low temperature environment, greatly limiting their application scenarios.^[2] Thus, exploring novel electrolytes with ultra-low freezing point is of great significant to broaden their application field in cold regions.

Numerous research investigations have been made to enhance the low-temperature electrochemical performance of ASIBs. One efficient strategy is to regulate the electrode materials, such as expanding interlayer spacing to promote Na^+ transfer, designing nanostructure to decrease the ionic migration distance, surface coatings with conductive carbon to

improve electronic conductivity and doping metal ions in electrodes to prevent structure collapse during cycling.^[3] However, these design philosophies were specially focused on the electrode modification, which cannot address the underlying problem for the high freezing point of aqueous electrolytes. Additionally, their improvement degrees for operating temperature and cyclic stability were often unsatisfactory, difficult to fulfill the requirements of most districts.^[4] Under these circumstances, the electrolyte modification strategy was a simple and practical design principle to fundamentally resolve the above bottle-neck interfacial challenges, because it can drastically lower the freezing point of ASIBs electrolytes. Some pioneering studies have achieved great progress by adding flammable and toxic organic solutions as cosolvents into aqueous electrolytes to lower their freezing point such as dimethyl sulfoxide and acetonitrile.^[5] Despite these modified electrolytes remain liquid under low temperature, their ionic conductivity would be greatly affected by the high viscosity and low polarity of organic cosolvents.^[6] Unsatisfactory, the aforementioned superiorities of ASIBs such as environmental friendliness and cost-effective would be remarkably decreased. In this consideration, exploring pure inorganic ASIBs electrolyte with ultra-low freezing point is considered to be an ideal choice.^[6c,7] Although the most frequently ASIBs electrolyte based on NaClO_4 salt has the lowest freezing point of -37°C when its concentration is $\sim 8.85 \text{ m}$ (m: mol kg^{-1}), the lower-temperature limit is still higher than that of many regions during winter on earth.^[8] More interestingly, introducing inorganic salt CaCl_2 as inert and anti-freezing additive for NaClO_4 based electrolyte can reduce its freezing point below -50°C and the ASIBs can efficiently work at -30°C .^[7a] However, the improvement degree was still undesirable. Based on these thorough considerations, it is necessary to design pure

[a] Dr. Y. Si
Logistics University of People's Armed Police Force
Tianjin 300309, China
E-mail: siyuch@163.com

[b] Dr. K. Zhu, Dr. Z. Sun, Dr. T. Jin, Dr. X. Chen, Prof. H. Li, Prof. L. Jiao
Key Laboratory of Advanced Energy Materials Chemistry
(Ministry of Education),
Renewable Energy Conversion and Storage Center (RECAST),
College of Chemistry, Nankai University
Tianjin 300071, China
E-mail: jiaolf@nankai.edu.cn

 Supporting information for this article is available on the WWW under
<https://doi.org/10.1002/batt.202200308>

 An invited contribution to a Special Collection dedicated to Aqueous Electrolyte Batteries.

inorganic electrolyte with ultra-low freezing point to boost the development of ASIBs with long-term cycling stability.

Herein, inorganic salt $\text{Mg}(\text{ClO}_4)_2$ was introduced as inert-support salt to decrease the freezing point of ASIBs electrolyte due to the high ionic potential of Mg^{2+} with strong polarization effect. ^1H nuclear magnetic resonance (NMR) and Raman results clearly revealed the original hydrogen-bonding network among water molecules was significantly destroyed by Mg^{2+} and the difficulty of ice formation was increased under subzero temperature. The high solubility NaClO_4 salt was selected to prepare the hybrid $3.5 \text{ m Mg}(\text{ClO}_4)_2 + 0.5 \text{ m NaClO}_4$ electrolyte possessing an ultra-low freezing point ($<-80^\circ\text{C}$) and a high ionic conductivity of 4.86 mS cm^{-1} at -60°C . With these merits, the active carbon | $\text{NaTi}_2(\text{PO}_4)_3 @ \text{C}$ batteries delivered an ultra-long

cycling stability of 20000 cycles under a current density of 10 C ($1 \text{ C} = 133 \text{ mA h g}^{-1}$) and remarkable rate capability at -50°C . Similar exceptional long-period performance of 10000 cycles under 8 C can be obtained when ASIBs was tested at -60°C , revealing the rapid reaction kinetics of this system under ultra-low temperature. Furthermore, some electronic devices including LED bulbs, smartphone and motor powered by ASIBs can also be continuously operated at -60°C .

Results and Discussion

From the phase diagram of $\text{Mg}(\text{ClO}_4)_2\text{-H}_2\text{O}$ system (Figure 1a), its freezing point was closely related to the $\text{Mg}(\text{ClO}_4)_2$

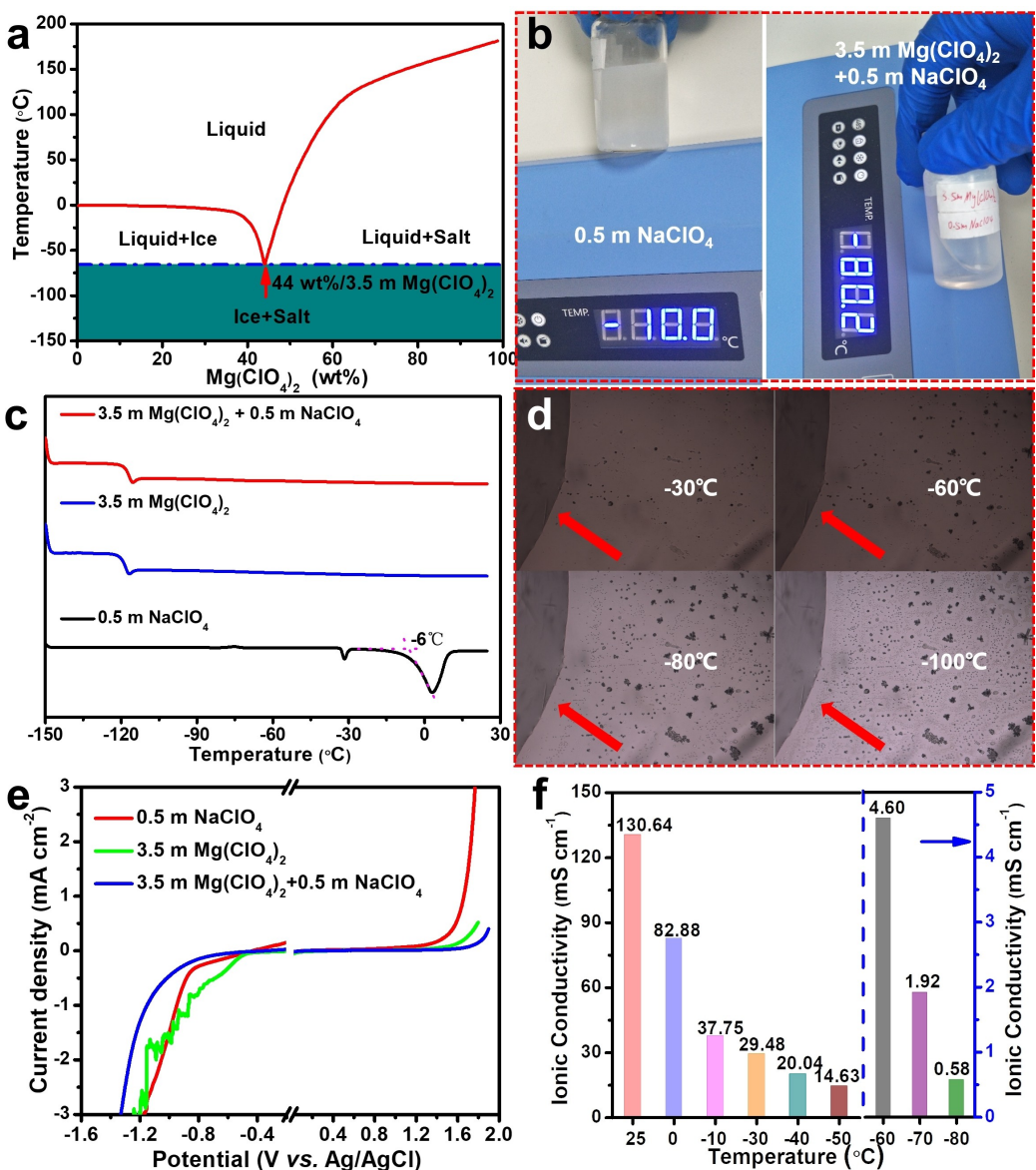


Figure 1. a) Phase diagram of $\text{Mg}(\text{ClO}_4)_2\text{-H}_2\text{O}$ system. b) The optical photograph of the 0.5 M NaClO_4 electrolyte at -10°C and the optical photograph of the $3.5 \text{ M Mg}(\text{ClO}_4)_2 + 0.5 \text{ M NaClO}_4$ electrolyte at -80°C . c) DSC results (from -150 to 30°C with a heating rate of 5°C min^{-1}) of various electrolytes. d) Polarizing microscope observation of the $3.5 \text{ M Mg}(\text{ClO}_4)_2 + 0.5 \text{ M NaClO}_4$ electrolyte during cooling process. e) The electrochemical stability window of different electrolytes obtained by cycling voltammetry. f) The ionic conductivity of $3.5 \text{ M Mg}(\text{ClO}_4)_2 + 0.5 \text{ M NaClO}_4$ electrolyte at different temperatures.

concentration. Upon the concentration increased, the freezing point decreased at first because the enhanced solvation effect of cation continuously changed the chemical environment of water molecules. With the further increase of $\text{Mg}(\text{ClO}_4)_2$, the boosted ion-pairs number obviously weakened the polarization effect under higher concentration and salt-extraction appeared under low temperature. When its content in the $\text{Mg}(\text{ClO}_4)_2\text{-H}_2\text{O}$ mixture was 44 wt% or its concentration was 3.5 m, the present system can achieve an optimal balance between concentration and freezing point with the lowest value of -69°C .^[8a,9] Thus, to overcome the above-mentioned limitation of the single NaClO_4 salt (Figure S1, Supporting Information), $\text{Mg}(\text{ClO}_4)_2$ with the deep-eutectic-point concentration (3.5 m) was selected as the supported salt to obtain lower freezing point for aqueous electrolyte. The frequently-used inorganic salt NaClO_4 with a low concentration (0.5 m) was selected to provide carriers during cycling due to its low cost and high solubility, which can simultaneously avoid the interference of anions. As a proof of concept, the hybrid 3.5 m $\text{Mg}(\text{ClO}_4)_2 + 0.5 \text{ m NaClO}_4$ electrolyte still remained liquid state under -80°C (Figure 1b), which was far below the lowest winter-temperature in most area on the earth.^[8b] Clearly, the 0.5 m NaClO_4 electrolyte was fully frozen at -10°C and the optical image of the 3.5 m $\text{Mg}(\text{ClO}_4)_2$ electrolyte was shown in Figure S2. Differential scanning calorimeter (DSC) was firstly used to estimate the freezing point of different electrolytes. For the hybrid 3.5 m $\text{Mg}(\text{ClO}_4)_2 + 0.5 \text{ m NaClO}_4$ electrolyte (Figure 1c), no obvious phase transition temperature was observed between -100 and 25°C . Its glass transition temperature was around -122°C , indicating the lower freezing points. In stark contrast, the freezing point of the 0.5 m NaClO_4 electrolyte was around -6°C , which agreed well with the observation results in Figure 1(b). As shown in Figure 1(d), no salting-out phenomenon or ice crystal appeared during cooling process for the hybrid electrolyte. By contrast, ice crystal formed for the 0.5 m NaClO_4 electrolyte under relatively high temperature (Figure S3). Thus, the hybrid electrolyte had a satisfactory freezing point as expected and can meet the requirements for ultra-low temperature ASIBs.

Electrochemical stable window (ESW) was one of the most important parameters for aqueous electrolyte owing to the narrow voltage window for water decomposition (1.23 V).^[10] As shown in Figure 1(e), the ESW of 0.5 m NaClO_4 electrolyte was only $\sim 2.1 \text{ V}$ when the current density of 0.2 mA cm^{-2} was defined as the minimum value for electrolyte decomposition.^[11] Although the hydrogen evolution voltage increased for the 3.5 m $\text{Mg}(\text{ClO}_4)_2$ electrolyte, its oxygen evolution voltage had improved and its ESW was $\sim 2.2 \text{ V}$. Compared to the above two electrolytes, both the hydrogen and oxygen evolution voltage for the hybrid 3.5 m $\text{Mg}(\text{ClO}_4)_2 + 0.5 \text{ m NaClO}_4$ electrolyte had improved and its ESW reached $\sim 2.68 \text{ V}$ due to the decreased content of free water molecules in this system, which was very close to the ESW of the common water-in-salt 17 m NaClO_4 electrolyte ($\sim 2.8 \text{ V}$), but the hybrid electrolyte had a relatively lower concentration and cost.^[12] The ionic conductivity for the 3.5 m $\text{Mg}(\text{ClO}_4)_2 + 0.5 \text{ m NaClO}_4$ electrolyte under different temperatures was plotted in Figure 1f. The hybrid electrolyte had a high ionic conductivity of $130.64 \text{ mS cm}^{-1}$ under room

temperature (25°C). Although it had a downward trend with the decrease of test temperature, 14.63 mS cm^{-1} was obtained at -50°C . When tested at -60°C , the hybrid electrolyte still had an acceptable level of ionic conductivity (4.60 mS cm^{-1}), which was higher than the reported low-temperature aqueous electrolytes when organic cosolvents were added.^[5a] Even at -80°C , an ionic conductivity of 0.58 mS cm^{-1} was surprisingly remained for the 3.5 m $\text{Mg}(\text{ClO}_4)_2 + 0.5 \text{ m NaClO}_4$ electrolyte. The ionic conductivity of 0.5 m NaClO_4 electrolyte (Figure S4) under 25 and 0°C were 76.86 and 30.54 mS cm^{-1} , both lower than that of the hybrid electrolyte due to its lower ionic concentration and higher freezing point. Thus, the hybrid electrolyte had a relatively wide ESW and high ionic conductivity under ultra-low temperature.

The anti-freezing mechanism for the hybrid electrolyte was firstly investigated by ^1H NMR method. As plotted in Figure 2(a), the ^1H peak for pure water sample located at $\sim 4.873 \text{ ppm}$. When NaClO_4 salt was added, the ^1H peak for the 0.5 m NaClO_4 electrolyte shifted to lower field due to the electron-withdrawing effect of cation and the relative chemical shift difference was $\sim 0.075 \text{ ppm}$. For the 3.5 m $\text{Mg}(\text{ClO}_4)_2$ electrolyte, its relative chemical shift difference was up to $\sim 0.159 \text{ ppm}$ due to Mg^{2+} had a higher ionic potential than Na^+ . The ^1H NMR peak for the 3.5 m $\text{Mg}(\text{ClO}_4)_2 + 0.5 \text{ m NaClO}_4$ electrolyte further shifted lower field and the relative chemical shift difference was $\sim 0.2 \text{ ppm}$, because both Mg^{2+} and Na^+ as hydrogen-bonded acceptors can coordinate with water molecules to change their chemical environment.^[2a,3b] More interestingly, the ^1H NMR peak for 3.5 m $\text{Mg}(\text{ClO}_4)_2 + 1 \text{ m NaClO}_4$ electrolyte shifted higher field compared to the 3.5 m $\text{Mg}(\text{ClO}_4)_2 + 0.5 \text{ m NaClO}_4$ electrolyte due to the stronger ion coupling effect under higher concentration.^[13] In addition, the salting out phenomenon appeared when the 3.5 m $\text{Mg}(\text{ClO}_4)_2 + 1 \text{ m NaClO}_4$ electrolyte was taken out from the -50°C environment (Figure S5) and the higher concentration salt would increase their viscosity under low temperature. The above discussion revealed that only the suitable concentration of salt can efficiently regulate the chemical environment of water molecules and reduce the freezing point of electrolytes. As shown in Figure 2(b), the pure water had a broad Fourier transform infrared (FTIR) spectroscopy peak between 3800 and 2800 cm^{-1} , corresponding to the vibration of hydroxyl group. When different salts were added, the absorption peak obviously became broader and the main peak gradually moved to lower wavenumber side, indicating a conspicuous increase proportion of coordination water and reduced content of free water. In other words, the random distribution of water molecules with naturally hydrogen bond network was dramatically altered, which was beneficial to lower the freezing point of electrolytes. The different broadened degree once again proved that Mg^{2+} had an apparent effect on the chemical environment of water molecules due to its higher ionic potential than that of Na^+ .

When water molecules was in liquid state, the natural vibration of water molecules was in the form of water clusters due to the intermolecular H-bond with the structure of short-range order in local region. With temperature reduced, the vibration frequency of water molecules gradually declined and

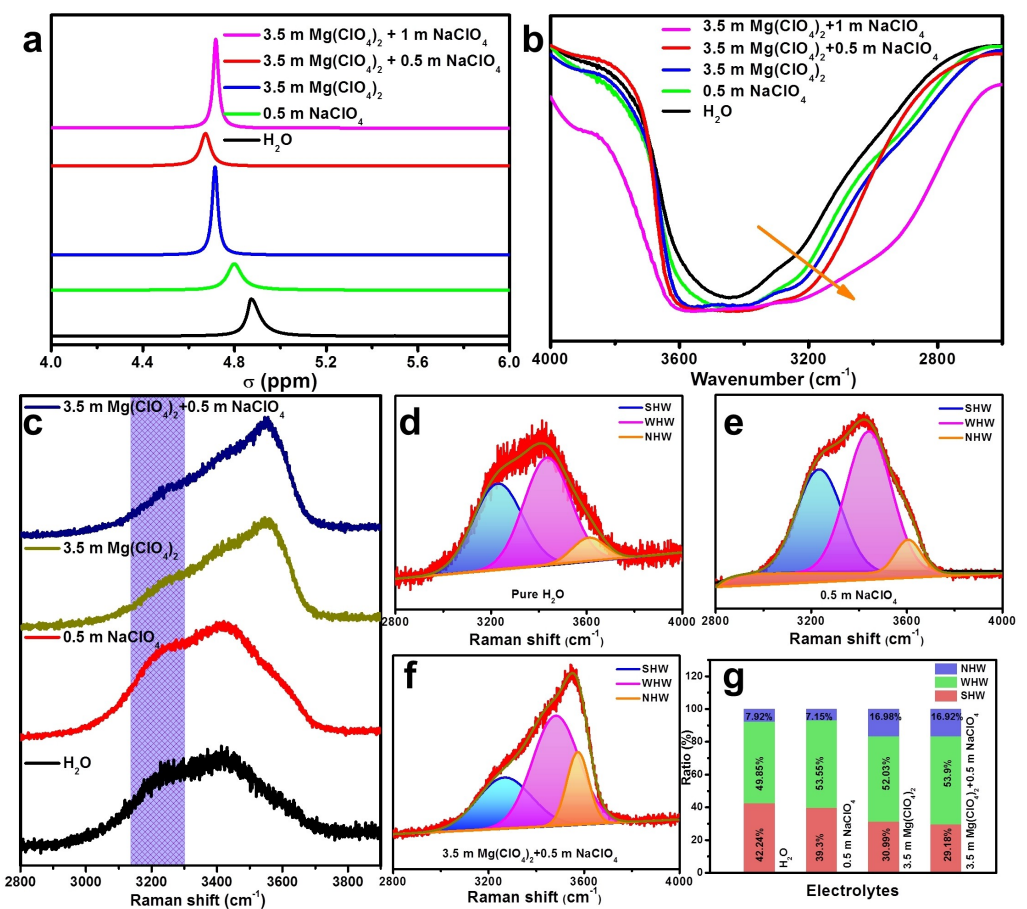


Figure 2. a) ^1H NMR results for various electrolytes. b) FTIR results for various electrolytes. c) Raman results for various electrolytes. The fitted Raman peaks: d) pure H_2O sample, e) 0.5 M NaClO_4 electrolyte and f) 3.5 M $\text{Mg}(\text{ClO}_4)_2 + 0.5 \text{ M NaClO}_4$ electrolyte. g) The component proportions of water with different hydrogen bond for various electrolytes.

water clusters grew. All the water molecules were limited by the intermolecular H-bond with the regular structure of long-range order below freezing point and ions cannot migrate freely, resulting in the premature failure of ASIBs under low temperature.^[3b,c] Theoretically speaking, one water molecule at most formed tetrahedral hydrogen bonds with the surrounding water molecules. Based on the coordinated hydrogen bond number, water molecules can be classified into three general types: strong hydrogen bond water (SHW) with four H-bonds, week hydrogen bond water (WHW) with one to three H-bonds and no hydrogen bond water (NHW) or free water molecules.^[5a,14] The intermolecular H-bond was in continual formation and decomposition due to the continual vibrations of water molecules and WHW was the major component in the liquid water. The formation of ice with long-range order structure was strongly associated with the proportion of SHW, because the water clusters can be regarded as the seed of ice crystal during the early period. Thus, reducing the content of SHW was an efficiently design principle to lower the freezing point of aqueous electrolyte.

From the Raman measurement results in Figure 2(c), the shoulder peaks in the lower wavenumber side corresponding to SHW for the pure water and 0.5 M NaClO_4 samples were

quite obviously. When $\text{Mg}(\text{ClO}_4)_2$ salt was added, the shoulder peaks faded away and the main Raman peaks gradually shifted higher wavenumber side for the 3.5 M $\text{Mg}(\text{ClO}_4)_2$ and 3.5 M $\text{Mg}(\text{ClO}_4)_2 + 0.5 \text{ M NaClO}_4$ electrolytes, indicating the drastically declined content of SHW in these systems.^[3a] After peak-differentiation-imitating for the Raman results (Figures 2d–g and S6), WHW was the main composition in the four different electrolytes as expected. The proportion of SHW was 39.3% for the 0.5 M NaClO_4 electrolyte, very close to that in the pure water sample (42.24%), which was related to its relatively high freezing point (Figure 1b and c). For the 3.5 M $\text{Mg}(\text{ClO}_4)_2$ electrolyte, the proportion of SHW was 30.99%, far lower than that of the above two samples and the electrolyte had an ultra-low freezing point (Figure 1a). More encouragingly, the 3.5 M $\text{Mg}(\text{ClO}_4)_2 + 0.5 \text{ M NaClO}_4$ electrolyte had the lowest proportion of SHW (29.18%), similar to the 3.5 M $\text{Mg}(\text{ClO}_4)_2$ electrolyte. Thus, the obviously decreased freezing point for the hybrid electrolyte was mainly ascribed to the higher ionic potential and stronger polarization effect of H-bond acceptor Mg^{2+} rather than Na^+ , which had more competitive advantage to acquire water molecules from water clusters, increase distance among water molecules and affect their local chemical environment (Figure 2a).

For the electrochemical measurements under low temperature, the common active carbon (AC) cathode and $\text{NaTi}_2(\text{PO}_4)_3@\text{C}$ (NTP@C) anode were used in this work to maximize the benefits of aqueous electrolyte, such as fast reaction kinetics.^[15] Their basic characterizations were displayed in Figures S7–S9. Prior to the electrochemical performance evaluations in the form of full ASIBs, both cathode and anode electrodes were measured in the form of three-electrode system under room temperature to confirm the role of charge carriers. As shown in Figure 3(a), no redox peaks can be observed from the cyclic voltammetry (CV) curves for the NTP@C anode when cycled in the 3.5 m $\text{Mg}(\text{ClO}_4)_2$ electrolyte, revealing Mg^{2+} cannot intercalate into the position for Na^+ in the host NTP@C, which can be further confirmed by the charge-discharge test. Almost no capacity was examined under 1 C when tested in the 3.5 m $\text{Mg}(\text{ClO}_4)_2$ electrolyte (Figure 3d). As a comparison, there was one pair obvious redox peaks in the CV curves for the NTP@C anode (Figure 3b), corresponding to the phase transition between $\text{NaTi}_2(\text{PO}_4)_3$ and $\text{Na}_3\text{Ti}_2(\text{PO}_4)_3$ due to the Na^+ insertion/extraction.^[16] However, the NTP@C anode delivered a poor cyclic stability when cycled in the 0.5 m NaClO_4 electrolyte under a current density of 5 C (Figure 3e), because the 0.5 m NaClO_4 electrolyte contained abundant free water molecules (Figure 2d and g). For the hybrid 3.5 m

$\text{Mg}(\text{ClO}_4)_2 + 0.5 \text{ m NaClO}_4$ electrolyte (Figure 3c), the NTP@C anode exhibited one pair similarly obvious redox peaks to that was cycled in the 0.5 m NaClO_4 electrolyte, demonstrating Na^+ was the real charge-carrier ions and Mg^{2+} was electrochemical inert for the NTP@C, which can be ascribed to the higher hydration energy ($-1922 \text{ kJ mol}^{-1}$) and larger hydration radius (4.28 Å) of Mg^{2+} than that of Na^+ (-405 kJ mol^{-1} and 3.58 Å), respectively.^[17] More encouragingly, the NTP@C anode delivered a satisfactory performance in the hybrid electrolyte system. As plotted in Figure 3(f), the NTP@C anode exhibited a high discharge specific capacity of 74.1 mAh g^{-1} under 5 C after 1000 cycles with no obvious capacity fading. For the aspect of AC cathode (Figure 3g–i), no obvious electrochemical differences were observed when cycled in the above three electrolytes under 2 C, because the energy storage mechanism of AC cathode was based adsorption/desorption of anion without phase transition process during cycling. The charge/discharge voltage-specific capacity curves of the electrodes at different current capacities under room temperature were exhibited in Figure S10. Thus, the full batteries can possess the advantage of rapid charge-discharge ability based the AC cathode and NASICON-type NTP@C anode and their electrochemical performance under room temperature was demonstrated in Figure S11.

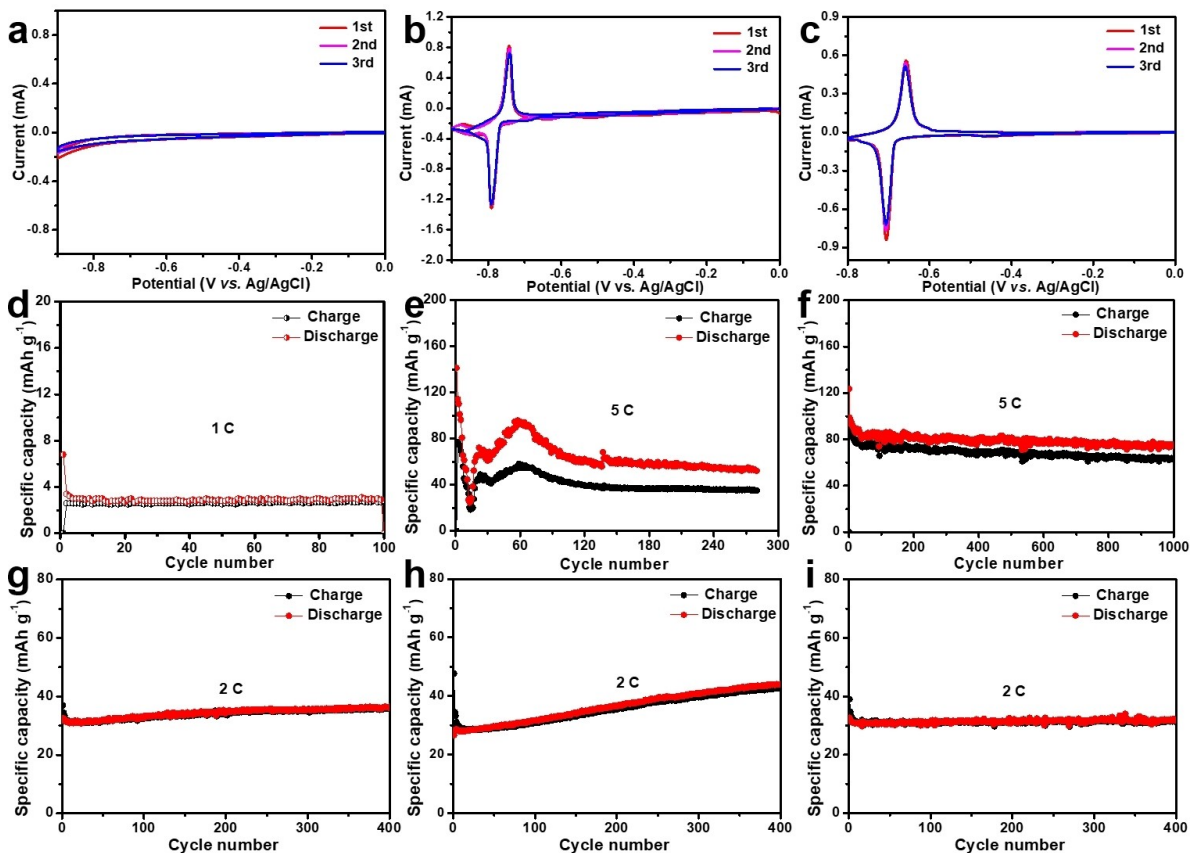


Figure 3. Cyclic voltammetry curves of the NTP@C sample at different electrolytes (V vs. Ag/AgCl): a) 3.5 m $\text{Mg}(\text{ClO}_4)_2$ electrolyte, b) 0.5 m NaClO_4 electrolyte and c) 3.5 m $\text{Mg}(\text{ClO}_4)_2 + 0.5 \text{ m NaClO}_4$ electrolyte. Cyclic performances of the NTP@C sample at different electrolytes: 3.5 m $\text{Mg}(\text{ClO}_4)_2$ electrolyte (1 C, d), 0.5 m NaClO_4 electrolyte (5 C, e) and 3.5 m $\text{Mg}(\text{ClO}_4)_2 + 0.5 \text{ m NaClO}_4$ electrolyte (5 C, f). Cyclic performances of the AC sample at different electrolytes under 2 C: g) 3.5 m $\text{Mg}(\text{ClO}_4)_2$ electrolyte, h) 0.5 m NaClO_4 electrolyte and i) 3.5 m $\text{Mg}(\text{ClO}_4)_2 + 0.5 \text{ m NaClO}_4$ electrolyte.

Figure 4 reflected the electrochemical performance of the full batteries when cycled under various current densities at -50°C . As shown in Figure 4(a), the full batteries delivered a high capacity of 52.33 mAh g^{-1} in the first cycle at 1 C. After 1000 cycles, the discharge specific capacity still reached 46.04 mAh g^{-1} with a capacity retention of $\sim 87.98\%$. Rate capabilities were tested at -50°C to intuitively investigate the rapid charge-discharge ability of the full batteries. As plotted in Figure 4(b), the full batteries delivered average discharge specific capacities of 59.53 , 55.98 , 50.73 , 47.08 , 44.29 and 42.03 mAh g^{-1} when cycled at 0.5 , 1 , 2 , 3 , 4 and 5 C, respectively. More critically, when the current density recovered to the initial 0.5 C, the capacity correspondingly returned to $\sim 59.44\text{ mAh g}^{-1}$, revealing its superior rate capabilities. The long-term cycling tests were further measured under larger current density. The full batteries possessed a high capacity of 41 mAh g^{-1} at 5 C and a capacity retention of $\sim 73.66\%$ after 10000 cycles under -50°C (Figure 4c). In addition, the full

batteries delivered a satisfactory capacity retention of $\sim 80.52\%$ after 20000 cycles when cycled at a higher current density of 10 C (Figure 4d), corresponding to an ultra-low capacity loss of $\sim 9.74 \times 10^{-4}\%$ for per cycle. Based on these admirable findings, this system exhibited an excellent electrochemical performance at -50°C .

In order to further evaluate the low temperature limit of this energy storage system, the full batteries were tested under -60°C , which was lower than most human activity region. As shown in Figure 5(a), the full batteries delivered a high capacity of 83.2 mAh g^{-1} under -60°C at the current density of 0.2 C with the initial coulombic efficiency of $\sim 78.86\%$. After 100 cycles, 66.9 mAh g^{-1} can be achieved with the capacity retention of 80.4% . The specific-capacity voltage curves in the initial cycles overlapped well (Figure 5b), demonstrating the remarkable reversibility of this system. More significantly, the full batteries exhibited a desirable capacity of 23.2 mAh g^{-1} after 10000 cycles under the current capacity of 8 C with the

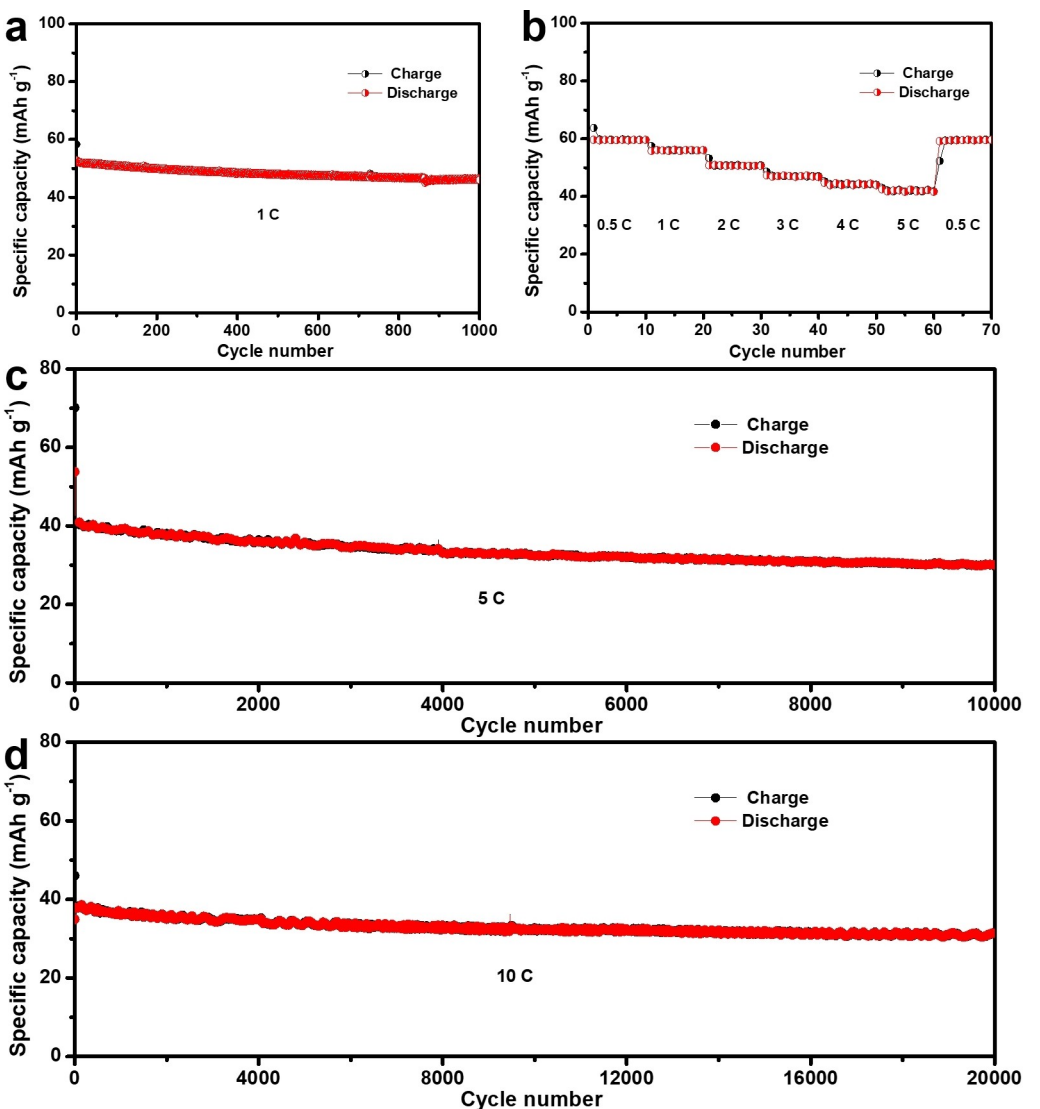


Figure 4. The electrochemical performance of the full batteries when tested under -50°C with different current density: a) 1 C, b) rate performances from 0.5 to 5 C, c) 5 C and d) 10 C.

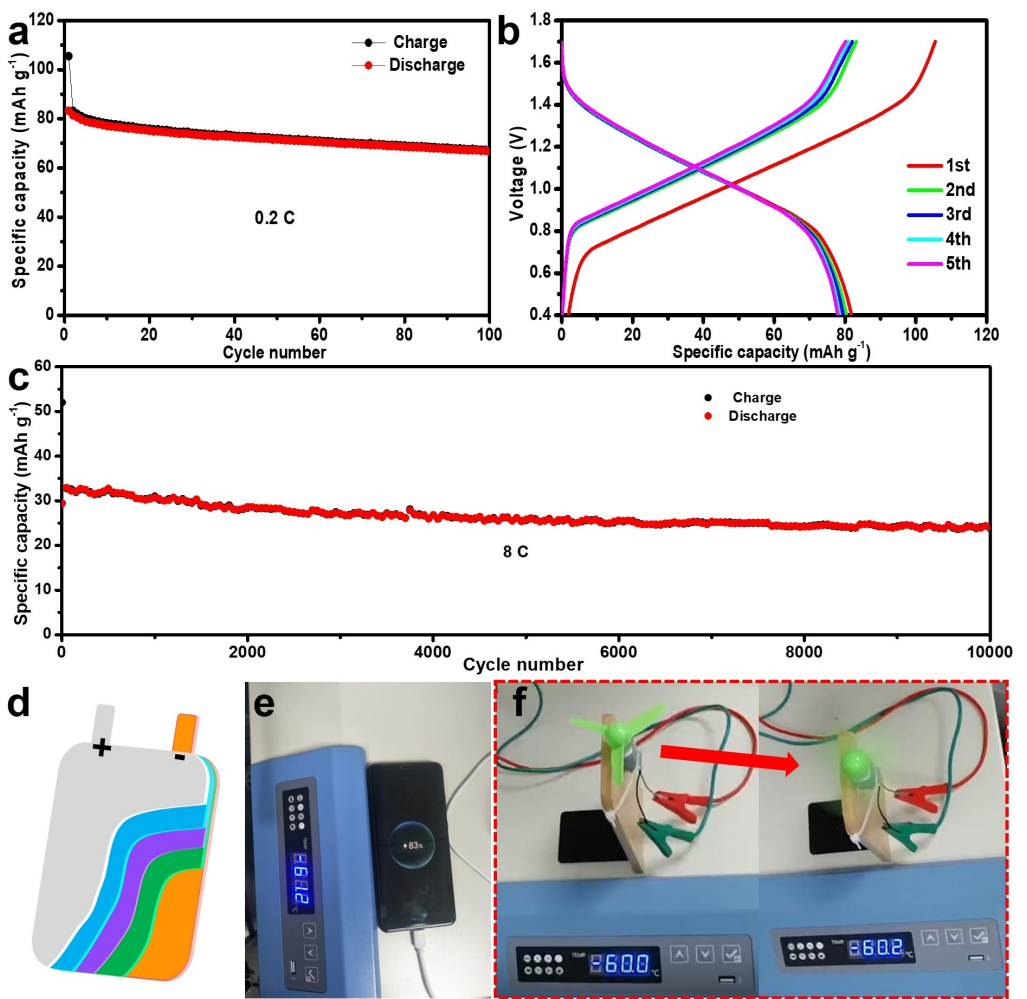


Figure 5. a) The electrochemical performance of the full batteries when tested under -60°C with a current density of 0.2 C. b) The charge/discharge voltage–specific capacity curves of the full batteries for the initial cycles under -60°C . c) Cyclic performances of the full batteries at 8 C under -60°C . d) The schematic of pouch cell. Exhibition of electronic devices powered by the pouch cells under -60°C : e) smart phone and f) motor.

capacity retention of 74.1% (Figure 5c). In addition, the electrochemical performance of full cells at different temperatures was presented in Figure S12. Figure S13(a) displayed the energy storage schematic of the system in the form of coin batteries. Two coin batteries connected in series can facilely light up 16 LED bulbs at -60°C (Figure S13b). Even at -70°C (Figure S13c), these bulbs were completely lit by coin batteries. Thus, this system possessed a satisfactory ultra-low temperature performance and application prospect.

Based on the above excellent results, pouch batteries were assembled in our lab to further explore the versatility of this system, which was closer to the demand of practical application than coin batteries. Figure 5(d) showed the schematic synthesis procedures of pouch batteries and Figure S14 displayed the optical image of our assembled pouch battery. As a comparison, the pouch cell used the same active materials and low-temperature electrolyte to the aforementioned coin battery. Thus, they shared the similar storage mechanism, which was beneficial to comprehensively evaluating the electrochemical performance of this system. When cycled under a current

density of 2 C at -60°C , the pouch batteries exhibited a high capacity of 31.1 mAh g^{-1} in the initial cycle. After 100 cycles, they still remained a capacity of 21.4 mAh g^{-1} with a capacity retention of $\sim 68.8\%$ (Figure S15). The aforementioned excellent electrochemical performance of the pouch batteries revealed that this energy storage system did not have an obvious capacity deterioration when the system was in amplified experiments. On this basis, three pouch batteries were interconnected together. As plotted in Figure 5(e), the pouch batteries packs can recharge our smartphone under -60°C , revealing an appealing prospect. As per our knowledge, this was the first report about recharging cellphone by ASIBs at -60°C , which was closer to our daily life rather than lighting up LED bulbs by aqueous ion batteries.^[14,18] To further explore the application limitation, a motor was used as a representative example in this work, which was started by a high power supply. As shown in Figure 5(f), the motor can be facilely operated at -60°C by this energy storage. The remarkable performance was mainly attributed to the $3.5\text{ M Mg(ClO}_4)_2 + 0.5\text{ M NaClO}_4$ electrolyte had a high ionic conductivity of

4.60 mS cm⁻¹ at -60 °C, which was the same level of organic electrolyte at room temperature. Another factor was the AC cathode and NTP@C anode had the intrinsic advantage of fast ion migration during cycling. Based on these thorough validations, this system displayed a great potential on real-world application under ultra-low temperature.

Conclusion

In summary, the novel 3.5 m Mg(ClO₄)₂ + 0.5 m NaClO₄ hybrid electrolyte with an ultra-low freezing point was firstly reported in this work. Various characterization techniques demonstrated that Mg²⁺ had an apparent influence on chemical environment of water molecules, efficiently attracted water from water clusters and modified the initial hydrogen-bonding network, subsequently lowering the freezing point of the electrolyte eventually. The hybrid electrolyte possessed a considerable ionic conductivity of 4.6 mS cm⁻¹ under -60 °C and the electrochemical measurements confirmed that Mg²⁺ was electrochemical inactive during cycling. Based on these advantages, the batteries can deliver a cyclic performance of 10000 cycles at 8 C with negligible capacity fading under -60 °C. Particularly, the pouch cells can recharge smartphone and drive a motor under -60 °C, exhibiting great potential in real life. With these breakthroughs, our feasible strategy paves the way to accelerate the development of high-power supply under ultra-low temperature and boosts the large-scale energy storage applications of aqueous batteries.

Supporting Information

Supporting Information is available from the online or from the authors.

Acknowledgements

This work was financially supported by the National Natural Science Foundation of China (52171228, 52025013, 52071184), the 111 Project (B12015), and the Fundamental Research Funds for the Central Universities.

Conflict of Interest

The authors declare no competing financial interest.

Data Availability Statement

Research data are not shared.

Keywords: aqueous sodium-ion batteries • excellent performance • magnesium perchlorate • ultra-low temperature

- [1] a) T. Liang, R. Hou, Q. Dou, H. Zhang, X. Yan, *Adv. Funct. Mater.* **2020**, 31, 2006749; b) T. Jin, X. Ji, P. Wang, K. Zhu, J. Zhang, L. Cao, L. Chen, C. Cui, T. Deng, S. Liu, N. Piao, Y. Liu, C. Shen, K. Xie, L. Jiao, C. Wang, *Angew. Chem. Int. Ed.* **2021**, 60, 11943; c) X. Tang, D. Zhou, B. Zhang, S. Wang, P. Li, H. Liu, X. Guo, P. Jaumaux, X. Gao, Y. Fu, C. Wang, C. Wang, G. Wang, *Nat. Commun.* **2021**, 12, 2857.
- [2] a) H. Wang, Z. Chen, Z. Ji, P. Wang, J. Wang, W. Ling, Y. Huang, *Mater. Today* **2021**, 19, 100577; b) C. Zhao, J. Liu, N. Yao, J. Wang, D. Ren, X. Chen, B. Li, Q. Zhang, *Angew. Chem. Int. Ed.* **2021**, 133, 15409; c) M. Peng, L. Wang, L. Li, Z. Peng, X. Tang, T. Hu, K. Yuan, Y. Chen, *eScience* **2021**, 1, 83.
- [3] a) A. Tron, S. Jeong, Y. Park, J. Mun, *ACS Sustainable Chem. Eng.* **2019**, 7, 14531; b) Y. Zhao, Z. Chen, F. Mo, D. Wang, Y. Guo, Z. Liu, X. Li, Q. Li, G. Liang, C. Zhi, *Adv. Sci.* **2020**, 8, 2002590; c) Z. Liu, X. Luo, L. Qin, G. Fang, S. Liang, *Advanced Powder Materials* **2022**, 1, 100011; d) S. Chen, Y. Zhang, H. Geng, Y. Yang, X. Rui, C. Li, *J. Power Sources* **2019**, 441, 227192.
- [4] a) Q. Nian, S. Liu, J. Liu, Q. Zhang, J. Shi, C. Liu, R. Wang, Z. Tao, J. Chen, *ACS Appl. Energy Mater.* **2019**, 2, 4370; b) J. Yin, C. Zheng, L. Qi, H. Wang, *J. Power Sources* **2011**, 196, 4080; c) D. Reber, R. Kühnel, C. Battaglia, *ACS Materials Lett.* **2019**, 1, 44.
- [5] a) Q. Nian, J. Wang, S. Liu, T. Sun, S. Zheng, Y. Zhang, Z. Tao, J. Chen, *Angew. Chem. Int. Ed.* **2019**, 131, 17150; b) Y. Sun, Y. Wang, L. Liu, B. Liu, Q. Zhang, D. Wu, H. Zhang, X. Yan, *J. Mater. Chem. A* **2020**, 8, 17998; c) Q. Dou, S. Lei, D. Wang, Q. Zhang, D. Xiao, H. Guo, A. Wang, H. Yang, Y. Li, S. Shi, X. Yan, *Energy Environ. Sci.* **2018**, 11, 3212.
- [6] a) W. Ye, H. Wang, J. Ning, Y. Zhong, Y. Hu, *J. Energy Chem.* **2021**, 57, 219; b) D. Xiao, Q. Dou, L. Zhang, Y. Ma, S. Shi, S. Lei, H. Yu, X. Yan, *Adv. Funct. Mater.* **2019**, 29, 1904136; c) L. Yan, J. Huang, Z. Guo, X. Dong, Z. Wang, Y. Wang, *ACS Energy Lett.* **2020**, 5, 685.
- [7] a) K. Zhu, Z. Li, Z. Sun, P. Liu, T. Jin, X. Chen, H. Li, W. Lu, L. Jiao, *Small* **2022**, 18, 2107662; b) Q. Zhang, K. Xia, Y. Ma, Y. Lu, L. Li, J. Liang, S. Chou, J. Chen, *ACS Energy Lett.* **2021**, 6, 2704; c) L. Yan, Y. Qi, X. Dong, Y. Wang, Y. Xia, *eScience* **2021**, 1, 212.
- [8] a) V. Chevrier, J. Hanley, T. Altheide, *Geophys. Res. Lett.* **2009**, 36, 10202; b) N. Chang, T. Li, R. Li, S. Wang, Y. Yin, H. Zhang, X. Li, *Energy Environ. Sci.* **2020**, 13, 3527.
- [9] a) T. Sun, S. Zheng, H. Du, Z. Tao, *Nano-Micro Lett.* **2021**, 13, 204; b) X. Bu, Y. Zhang, Y. Sun, L. Su, J. Meng, X. Lu, X. Yan, *J. Energy Chem.* **2020**, 49, 198.
- [10] K. Zhu, Z. Li, T. Jin, L. Jiao, *J. Mater. Chem. A* **2020**, 8, 21103.
- [11] a) Q. Dou, Y. Lu, L. Su, X. Zhang, S. Lei, X. Bu, L. Liu, D. Xiao, J. Chen, S. Shi, X. Yan, *Energy Storage Mater.* **2019**, 23, 603; b) H. Bi, X. Wang, H. Liu, Y. He, W. Wang, W. Deng, X. Ma, Y. Wang, W. Rao, Y. Chai, H. Ma, R. Li, J. Chen, Y. Wang, M. Xue, *Adv. Mater.* **2020**, 32, 2000074.
- [12] a) D. Choi, S. Lim, D. Han, *J. Energy Chem.* **2021**, 53, 396; b) D. Debanjana, P. Seeraj, *ACS Sustainable Chem. Eng.* **2020**, 8, 10613; c) M. Lee, S. Kim, D. Chang, J. Kim, S. Moon, K. Oh, K. Y. Park, W. Seong, H. Park, G. Kwon, B. Lee, K. Kang, *Mater. Today* **2019**, 29, 26.
- [13] D. Xiao, L. Zhang, Z. Li, H. Dou, X. Zhang, *Energy Storage Mater.* **2022**, 44, 10.
- [14] Q. Zhang, Y. Ma, Y. Lu, L. Li, F. Wan, K. Zhang, J. Chen, *Nat. Commun.* **2020**, 11, 4463.
- [15] a) J. Liang, K. Fan, Z. Wei, X. Gao, W. Song, J. Ma, *Mater. Res. Bull.* **2018**, 99, 343; b) Z. Li, D. Young, K. Xiang, W. Carter, Y. Chiang, *Adv. Energy Mater.* **2013**, 3, 290.
- [16] a) B. Zhao, B. Lin, S. Zhang, C. Deng, *Nanoscale* **2015**, 7, 18552; b) Z. Liu, Y. An, G. Pang, S. Dong, C. Xu, C. Mi, X. Zhang, *Chem. Eng. J.* **2018**, 353, 814; c) S. Wu, L. Wang, Y. Jiang, H. Yang, Y. Wu, Y. Yao, X. Wu, Y. Yu, *ACS Energy Lett.* **2022**, 7, 632.
- [17] B. Xiao, *Carbon Energy* **2020**, 2, 251.
- [18] a) F. Yue, Z. Tie, S. Deng, S. Wang, M. Yang, Z. Niu, *Angew. Chem. Int. Ed.* **2021**, 60, 1; b) W. Viola, T. Andrew, *J. Phys. Chem. C* **2020**, 125, 246.

Manuscript received: July 4, 2022
Revised manuscript received: August 8, 2022
Accepted manuscript online: September 1, 2022
Version of record online: September 19, 2022